6-20-2013

Reliability-based Design Optimization of Concrete Flexural Members Reinforced with Ductile FRP Bars

Bashar Behnam
Broome College, Binghamton, NY

Christopher D. Eamon
Wayne State University, Detroit, MI, christopher.eamon@wayne.edu

Reliability-Based Design Optimization of Concrete Flexural Members Reinforced with Ductile FRP Bars

Bashar Behnam[1] and Christopher Eamon[2]

ABSTRACT

In recent years, ductile hybrid FRP (DHFRP) bars have been developed for use as tensile reinforcement. However, initial material costs regain high, and it is difficult to simultaneously meet strength, stiffness, ductility, and reliability demands. In this study, a reliability-based design optimization (RBDO) is conducted to determine minimum cost DHFRP bar configurations while enforcing essential constraints. Applications for bridge decks and building beams are considered, with 2, 3, and 4-material bars. It was found that optimal bar configuration has little variation for the different applications, and that overall optimized bar cost decreased as the number of bar materials increased.

Keywords: FRP; reinforcement; concrete; reliability; optimization; RBDO

[1] Assistant Professor, Dept. of Civil Engineering Technology, Broome College, Binghamton, NY 13905.
[2] Associate Professor, Dept. of Civil and Environmental Engineering, Wayne State University, Detroit, MI 48202.
Corresponding author, email: eamon@eng.wayne.edu

1. Introduction

The maintenance costs associated with steel reinforcement corrosion are significant, with an estimated repair cost to bridges in the United States (US) alone estimated to be over $8 billion [1]. Not only do the corroding steel bars lose tensile capacity, potentially requiring strengthening or replacement, but the surrounding concrete is damaged as well, as it cracks as spalls due to expansion of the steel [2]. Various methods have been considered in an attempt to solve this problem, including adjusting the concrete mix design or increasing concrete cover to limit the penetration of corrosive chlorides; cathodic protection; and the use of galvanized, stainless steel, or epoxy-coated reinforcement [1, 2]. Another avenue of investigation is the use of fiber reinforced polymer (FRP) materials, which have been used in a small number of bridges around the world, as well as in the US, in the last two decades [3].

The federally-mandated specification for highway bridge design in the US, the American Association of State and Highway Transportation Officials (AASHTO) *Bridge Design Specifications* [4], does not directly address the use of FRP reinforcement. Nor does the American Concrete Institute *Building Code Requirements for Structural Concrete*, *ACI-318* [5]. However, special publications by AASHTO as well as ACI are available that directly address the use of FRP: the *ACI Guide for the Design and Construction of Structural Concrete Reinforced with FRP Bars, ACI-440.1R* [6], as well as the *AASHTO LRFD Bridge Design Guide Specification for GFRP-Reinforced Concrete Bridge Decks and Traffic Railings* [7], although the latter is specifically limited to glass FRP. Various other international codes and standards address FRP reinforcement as well, including the *Canadian Highway Bridge Design Code, CAS-S6-06* [8]; *the International Federation for Structural Concrete Bulletin 40* [9];

Recommendations provided by the Japan Society of Civil Engineers [10], the British Standards Institution [11], as well as others [12, 13].

Despite the availability of these design guides as well as the use of FRP reinforcement materials in bridge structures for over two decades, the use of FRP for reinforcement, as a replacement to traditional steel, is extremely limited in the US. This is due to several reasons, including a lack of familiarity among bridge designers; higher initial cost than steel; and lack of reinforcement ductility. Other potential drawbacks with FRP have discouraged use as well, such as a low tensile stiffness, inadequate bond, and degradation in alkaline environments, although these problems have been addressed with appropriate material choices and manufacturing processes [14].

Two remaining major challenges with FRP are lack of ductility and high cost. Low ductility is a difficult problem to overcome, as FRP bars are generally linear-elastic under load until tension rupture. This behavior may not only render an impending overload failure more difficult to detect, but may also limit the possibility of moment redistribution in indeterminate structures. In the last two decades, however, various researchers have developed FRP bar designs with significant ductility [15-22]. The majority of these designs are based on a hybrid concept, where the bar is made of several different FRP materials, each with a different ultimate strain. As the level of strain increases in the bar, the different fibers incrementally fail at their corresponding ultimate strains, reducing stiffness as the load on the bar is increased. With proper selection of materials and volume fractions, a highly ductile response can be obtained while maintaining sufficient tensile capacity, thus producing a ductile hybrid FRP (DHFRP) bar. Moreover, concrete flexural members reinforced with DHFRP bars have developed moment-curvature responses similar to that of corresponding steel-reinforced members [16, 14].

With regard to cost, although FRP bars are generally 6-8 times more expensive than steel reinforcement initially (with an entire bridge structure cost from about 25-75% higher if all steel reinforcement is replaced with FRP), life-cycle cost analysis of FRP-reinforced bridges demonstrated significant cost savings over similar steel-reinforced bridges throughout a 50 to 75 year bridge lifetime, due to expected decreases in maintenance costs [3]. The same study found that the FRP-reinforced bridge typically had roughly one-half or less of the total life-cycle cost of the corresponding steel-reinforced bridge, with cost savings usually beginning close to year 20 of the bridge service life. However, with an expected 20-year pay-back period, initial cost is still a major concern, and any initial cost savings are clearly highly desirable.

The reliability of structures reinforced with DHFRP bars is also a concern. To develop appropriate load and resistance factors for structural design, a reliability analysis, in the context of a code calibration, is generally needed. Such structural reliability analyses have been conducted for a wide range of FRP materials, including non-ductile FRP bars used in reinforced concrete flexural members [23, 24], as well as externally-bonded, non-ductile FRP used to strengthen concrete beams [25-32]. Just recently, however, has the structural reliability of concrete sections reinforced with DHFRP bars been analyzed, with only one study presented in the literature [33]. For the DHFRP-reinforced members considered in that study, it appeared that if DHFRP bars were designed using the *ACI 440.1R* resistance factors that were developed for (single material) non-ductile FRP bars, DHFRP-reinforced beam reliability was adequate, with reliability indices slightly higher than code target levels. However, the safety margin was not large, and if a different DHFRP bar configuration is considered, reliability may be inadequate.

Therefore, developing FRP-reinforced sections that can meet strength, ductility, stiffness, as well as reliability requirements, while minimizing cost, is difficult with a typical trail and

error design process, as the interaction of these various design requirements with DHFRP bar construction parameters is complex. In this paper, a reliability-based design optimization (RBDO) process is presented and applied to the development of DHFRP-reinforced concrete flexural members. The goal is to minimize (initial) material cost while meeting all required design constraints, primarily by selection of optimal bar construction parameters.

2. DHFRP-Reinforced Flexural Member Analysis

A general DHFRP bar cross-section is given in Figure 1. Here, the different fibers are placed in concentric layers, but various other configurations are possible, including winding, braiding, and symmetrically-distributed bundled arrangements [16, 14]. Typical analytical stress-strain curves for several DHFRP bar configurations are given in Figure 2, where the behavior of 2, 3, and 4-material bars (*B1-B3*, respectively) are shown. The resulting discontinuous stress-strain response closely resembles the experimental results found [16-18].

When DHFRP bars are used as tensile reinforcement in concrete flexural members, an expression for moment capacity can be developed as:

$$M_c = \left[d - K_2 \frac{\varepsilon_{f_1}}{K_1 \cdot f_c' \cdot b} \left(\sum_{i=1}^{n} v_{f_i} E_{f_i} + v_m E_m \right) \left(\sum_{i=1}^{n} v_{f_i} + v_m \right) A_T \right] \cdot \left[\varepsilon_{f_1} \left(\sum_{i=1}^{n} v_{f_i} E_{f_i} + v_{f_m} E_{f_m} \right) \left(\sum_{i=1}^{n} v_{f_i} + v_m \right) A_T \right] \quad (1)$$

In eq (1), M_c is calculated based on the first FRP material failure in the DHFRP bar, and this moment is taken as the nominal capacity M_n of the section. The first square bracketed term is the distance between the concrete compressive block and reinforcement centroids, while the second square bracketed term is the force in the reinforcement bar at first material failure. In both bracketed terms, $\sum_{i=1}^{n} v_{f_i} E_{f_i} = v_{f_1} E_{f_1} + v_{f_2} E_{f_2} + \cdots + v_{f_n} E_{f_n}$, where n is the number of fiber layers,

and v_{f_i} and E_{f_i} are the volume fraction and Young's modulus of fiber in layer *i*, respectively. Similarly, E_m and v_m are the Young's modulus and volume fraction of the resin, respectively, while ε_{f_1} is the failure strain of the first fiber type to fail, and A_T is the total area of the DHFRP tensile reinforcement. In the upper square bracketed term, f_c' is concrete compressive strength and K_1 and K_2 are parameters used to define the parabolic shape of the concrete compression block in Hognestad's nonlinear stress-strain model, where K_1 is the ratio of average concrete stress to maximum stress in the block and K_2 defines the location of the compressive block centroid [34]; *d* is the distance from the tension reinforcement centroid to the extreme compression fiber in the beam, and *b* is the width of the concrete compression block. Here it is assumed that the exterior fibers of the bar are ribbed or otherwise adequately roughened for adequate bond [35]. A simpler version of eq. (1) can be developed by using the Whitney model for the shape of the concrete stress block, with no significant difference in ultimate capacity results. However, the Hognestad model is required to evaluate cracked section response at load levels below ultimate, in order to generate the moment-curvature diagrams needed to evaluate section ductility, and was thus considered throughout this study.

For DHFRP-reinforced flexural members, ductility is a primary concern. When FRP is used as tension reinforcement, ductility index can be calculated from the corresponding load deflection or moment-curvature relationship using [36]:

$$\mu_\phi = \frac{\phi u}{\phi y} = \frac{1}{2}\left(\frac{E_{\text{total}}}{E_{\text{elastic}}} + 1\right) \tag{2}$$

where ϕ_u is ultimate curvature and ϕ_y is yield curvature (i.e. curvature at first DHFRP bar material failure), while E_{total} is computed as the area under the load displacement or moment-curvature diagram and E_{elastic} is the area corresponding to elastic deformation.

For this study, the minimum acceptable ductility index is taken as 3.0 [37, 38], which is similar to that for corresponding members reinforced with steel. As noted earlier, DHRFP bar ductility results from a sequence of non-simultaneous material failures with the condition that after a material fails, the remaining materials have the capacity to carry the tension force until the final material fails, to produce the desired ductility level in the concrete flexural member. Moreover, before the desired level of ductility is reached, each bar material must fail before the concrete crushes in compression (at an ultimate strain taken as $\varepsilon_{cu} = 0.003$).

To evaluate ductility, the moment-curvature diagram of the DHFRP-reinforced flexural member is needed, not just the nominal moment capacity given by eq. (1). For moment-curvature analysis, moment capacity up to concrete cracking is calculated based on the elastic section as $M_{cr} = f_r I_g / y_t$, where f_r is the concrete modulus of rupture, I_g is the uncracked section moment of inertia, and y_t the distance from the section centroid to the extreme tension fiber. For the cracked section, the relationship between internal strains and the resulting moment couple is developed based on the modified Hognestad model describing the nonlinear concrete stress-strain relationship. The resulting resisting moment is then determined by: $M = C_c\left(d - K_2 c\right)$ where C_c is the compressive force in the concrete and c is the distance from the top of the concrete compression block to the neutral axis, with parameters d and K_2 defined above. The corresponding curvature ϕ_c is then calculated as $\phi_c = \varepsilon_c / c$, where ε_c is the concrete strain at the top of the concrete compression block. For the development of the moment-curvature relationship, it is conservatively assumed that once the failure strain of a particular DHFRP bar material is reached, the affected material throughout the length of the flexural member immediately loses all load-carrying capability. This results in jagged moment-curvature diagrams, examples of which are shown in Figures 3-6. Note that at the peaks in the diagram,

two different values of moment capacity are theoretically associated with the same value of curvature. This occurs because once the most stiff existing material in the bar breaks, the cracked section stiffness decreases significantly and less moment is required to deform the beam the same amount. Actual experimental results of DHFRP-reinforced beams have shown smoother curves, closer to that constructed by drawing a line between the peaks and excluding the capacity drops shown in the Figures [14, 16]. However, including these theoretical low capacity points results in the most conservative ductility indices computed for sections reinforced with DHFRP bars, and this method is thus used to enforce the ductility constraint imposed in this study.

Due to the lower elastic modulus of many composite reinforcement materials as compared to steel, the possibility of excessive deflections must be considered. This concern is recognized in *ACI 440.1R*, where recommended limits on span/depth ratios for FRP-reinforced concrete flexural members are given. The estimation of flexural deflections in reinforced-concrete members becomes challenging, since the degree of cracking, and corresponding loss of stiffness, generally varies along the length of the flexural member. To account for this, various methods are available, one of which is presented by Branson [39, 40], which develops the effective moment of inertia I_e to be used for deflection calculation as:

$$I_e = \left(\frac{M_{cr}}{M_a}\right)^3 \beta_d I_g + \left[1 - \left(\frac{M_{cr}}{M_a}\right)^3\right] I_{cr} \le I_g \qquad (3)$$

where M_{cr} is the cracking moment, M_a is the applied moment, and β_d is a reduction factor to account for the typical lower stiffness associated with FRP reinforcing and potential bonding problems. To estimate deflections in this study, β_d is calculated as $\beta_d = 3.3\frac{I_{cr}}{I_g}$ [41], where I_g and I_{cr} are gross and cracked moment of inertias, respectively.

Although various factors affect DHFRP bar cost, the primary influence is that of the material itself. Manufacturing costs may also be significant, but as DHFRP bars have yet to be mass produced for commercial use, there is no readily available product manufacturing cost data available. Thus in this study, comparisons between DHFRP bar types are made based on material cost, which is computed as specific cost *sc*, as a proportion of DHFRP bar cost to that of traditional steel bars:

$$sc = \frac{C_f \, \rho_f}{C_s \, \rho_s} \tag{4}$$

where C_f is the cost of fiber material per unit weight, ρ_f is the density of the fiber, C_s is the cost of steel, and ρs is steel density. The specific costs of the materials considered in this study are given in Table 1, as taken from the available literature [14, 42, 43].

3. RBDO

In the RBDO process, inherent uncertainties associated with material properties and applied loads are captured in the mathematical formulation and solution of the optimization problem. There are multiple ways of formulating an RBDO problem [44-49]. In general, the procedure aims to establish the vector of design variables $\boldsymbol{Y} = \{Y_1, Y_2, ..., Y_{NDV}\}^T$ that would

$$\text{min} \quad f(\boldsymbol{X}, \boldsymbol{Y}) \tag{5}$$

$$\text{s. t.} \quad \beta_{gi}(X, Y) \geq \beta_{\min}; \; i = 1, N_p$$

$$D_j(\overline{X}, Y) \geq D_{\min}; \; j = 1, N_d$$

$$Y_k^l \leq Y_k \leq Y_k^u; \qquad k = 1 \text{ to } NDV$$

where $f(\boldsymbol{X}, \boldsymbol{Y})$ is the objective function of interest with dependence on design variables $\boldsymbol{Y}$ (DVs) and random variables (RVs) $\boldsymbol{X} = \{X_1, X_2, ..., X_n\}^T$, subjected to N_p probabilistic

constraints β_{gi} and N_d deterministic constraints D_j, where the resulting set of variables ($\boldsymbol{X,Y}$) must produce constraint evaluations that equal or exceed the minimum required probabilistic and deterministic limits, $\beta_{\min}$ and $D_{\min}$, respectively. Here, the probabilistic constraints are written in terms of generalized reliability index β, commonly used in structural reliability analysis in lieu of failure probability p_f directly. Each reliability index calculated is particular to an individual limit state g considered for probabilistic evaluation, and is in general a function of both RVs and DVs. Deterministic constraints may also be present in the RBDO problem. In this case, deterministic constraints are a function of DVs and RVs, but not full RV information. Here, variance (and higher moments) describing RV uncertainty do not affect deterministic calculations, and thus only RV magnitude is relevant, generally in the form of mean value ($\overline{X}$). Note that the sets of DVs and RVs may, and often do, overlap. In such cases the RV mean value changes during the optimization, as it is taken as the DV value. DVs are also often subjected to limits to prevent physically impractical solutions, with the kth design variable, Y_k limited by its lower and upper bounds, Y_k^l and Y_k^u, respectively.

DHFRP-reinforced section cost minimization is the RBDO problem of interest to this study, resulting in:

$$\text{min} \quad f(\boldsymbol{X},\boldsymbol{Y}) = A_{FRP}\sum_{i=1}^{n} sc_i v_i \tag{6}$$

$$\text{s.t.} \quad \beta_g \geq \beta_T$$

$$\phi M_n \geq M_u$$

$$\mu_\phi \geq \mu_L$$

$$\Delta \leq \Delta_L$$

$$M_{i+1} \geq M_i \,;\; i = 1 \text{ to } n\text{-}1$$

$$\sum_{i=1}^{n} v_i = 1.0$$

$$\varepsilon_n \geq k\varepsilon_{ult\ n}$$

where A_{FRP} is the total cross-sectional area of the DHFRP reinforcement in the section, sc_i is the specific cost of material i, and v_i is the volume fraction of material i of n total materials used in the reinforcing bar construction (here it is assumed that multiple DHFRP tension reinforcing bars used in a given beam are identical). Note that the cost of the concrete in the sections considered is negligible compared to the DHFRP reinforcement cost and is thus not included in f for simplicity. In this problem, a single probabilistic constraint β_g is of interest, which corresponds to the limit set by the minimum target reliability index β_T for structures designed to the relevant code standard, which is β_T =3.5 for both *ACI-318* and *AASHTO LRFD* as considered in this study [45, 51]. The critical deterministic constraints include requirements for the code-specified design capacity ϕM_n to meet the design load effect M_u, as well as an appropriate ductility limit μ_L , taken as 3.0, as discussed above, and a beam deflection limit Δ_L, taken as L/240 for FRP-reinforced sections, per *ACI 440.1R*. It is also desirable that the moment capacity of the section does not fall below the code-required capacity throughout the curvature range in which ductility is measured; hence a constraint is provided requiring successive moment capacity peaks M_{i+1} resulting from n material failures to not fall below that generated from a previous material failure. Also needed is a constraint ensuring that the resulting DHFRP bar geometry is physically possible; i.e. that the total of the material volume fractions in the bar equals unity. Finally, a constraint is imposed that is not theoretically necessary but included because it was found that it frequently results in ductility indices greater than the minimum

required. This involves limiting the strain in the last material to fail in the DHFRP bar to be no less than a fraction (k) of its failure strain at ultimate section failure (i.e. when concrete crushes in the compression zone), where k is taken to be 0.85. Imposing this constraint tends to increase ductility by providing greater reinforcement strains at ultimate capacity. Depending on the specific problem, imposing a higher k value than 0.85 is sometimes possible, but often results in an infeasible solution. An alternative to imposing this last constraint would be to formulate a multi-objective RBDO, minimizing cost while simultaneously maximizing ductility, but this is a substantially more numerically complicated and computationally costly problem to solve. Design variables are given in Table 2. Lower and upper DV bounds for concrete strength and member dimensions were selected to provide a range of design possibilities deemed reasonable for the applications considered (see *Flexural Members Considered*). As it is very difficult to chose an initial set of DV values that satisfies the imposed constraints (i.e. eq. 6), material volume fractions v and reinforcement area A_{FRP} were initially set to arbitrarily low values (the lower DV bounds) to begin the RBDO. Note that these initial DV values do not constitute a feasible design.

To evaluate the probabilistic constraint β_g, critical RVs affecting moment capacity must be identified. Flexural member resistance RVs relevant to all cases include manufacturing variations in volume fractions (v) of the different fibers types and resin used in the bar construction; modulus of elasticity (E) for the materials and resin; failure strain of the first material to fail (ε_{f_1}) (the only failure strain value which affects calculation of moment capacity); compressive strength of the concrete (f_c'); depth of reinforcement (d); and professional factor (P), which represents the ratio of the actual capacity to the theoretically-predicted capacity of the flexural member. For the building beam cases, width of the beam (b) is also taken as a RV. The

coefficient of variation, V, bias factor λ (ratio of mean to nominal value), and distribution type for each resistance RV are given in Table 3. Although a variety of RV data are presented in the literature, RV statistical parameters used in this study are selected for consistency with previous reliability-based code calibrations. Here, load and resistance RVs for the building beam are taken as those used to calibrate the *ACI 318* Code [51]; while bridge deck load and resistance data are taken as those used for the *AASHTO LRFD* Code calibration [50]; and FRP RV statistical parameters are taken from those used for the *ACI 440.1R* calibration [23], as well as from [53]. For the bridge slab, the load RVs considered are dead load of the slab (*DS*), wearing surface (*DW*), and parapets (*DP*), and truck wheel live load (*LL*); while for the building beam, load RVs are dead load (*DL*) and transient live load (50-year maximum). These values are shown in Table 4.

For reliability analysis, the relevant limit state g is: $g = M_c - M_a$, where M_c is the moment capacity of the section, as given by eq. 1, as a function of the resistance RVs given in Table 3, and M_a is the applied moment effect, as a function of the dead and live load RVs given in Table 4. In the RBDO, Monte Carlo simulation (MCS) was used to calculate probability of failure p_f associated with the limit state for each of the sections considered (see above), which was then transformed to reliability index β using $\beta = -\Phi^{-1}(p_f)$. The number of simulations was increased until β convergence was achieved. In general, this occurred close to 1×10^6 simulations.

4. Flexural Members Considered

In this study, three DHFRP bar concepts are considered in the RBDO process: 2, 3, and 4-material bars composed of continuous fibers, designated *B1*, *B2*, and *B3*, respectively. Table 1

provides the material choices considered, where Young's modulus (E) and ultimate strain (ε_u) are given.

For the RBDO problem, two typical tension-controlled reinforced concrete flexural member applications are considered; a bridge deck and a building floor beam. The bridge deck (Figure 7) is optimized over girder spacings of 1.8 and 2.7 m (6 and 9 ft), with 25 mm (1 in) cover for the DHFRP bars, placed in the top and bottom of the slab, as used in two FRP-reinforced bridge decks built in Wisconsin [54, 35]. Note that *AASHTO GFRP* [7] allows a minimum of 19 mm (¾ in) cover for a slab reinforced with composite bars. The bar diameter considered was 22 mm (7/8 in). The deck is designed to meet the flexural strength requirements of the *AASHTO LRFD Specifications* [4], using the equivalent strip method to determine required capacity for positive and negative slab moments. The relevant flexural design equation is: $\phi M_n = \gamma_{DC} M_{DC} + \gamma_{DW} M_{DW} + 1.75 M_{LL+IM}$, where resistance factor ϕ is taken as 0.55 (per *AASHTO GFRP* as well as *ACI 440.1R*); M_{DC} and M_{DW} refer to the moments caused by the deck self weight and wearing surface (taken as 75 mm (3 in) for a 13 mm (0.5 in) existing integrated surface and 62 mm (2.5 in) for future allowance), respectively; γ_{DC} are γ_{DW} are load factors that vary from 1.25 to 0.9, and 1.5 to 0.65, respectively, to generate maximum load effect; and M_{LL+IM} is the live load moment caused by the worst-case positioning of 72 kN (16 kip) truck wheel loads on the slab, in addition to a specified impact factor of 1.33. For the DHFRP bars, it is preferable that the carbon layer is placed on the exterior of the bar to protect the inner glass layers from alkaline attack in a cementitious environment. This results in use of an environmental factor C_E, which reduces bar design strength to account for potential material degradation, as 0.9, as recommended in *ACI 440.1R*.

For the building beam, two span lengths, 6 and 9.1 m (20 and 30 ft), were considered for optimization. Simple-span members were used, although a continuous member does not significantly alter results. The relevant flexural design equation is $\phi M_n = 1.2M_{DL} + 1.6M_{LL}$, where ϕ is 0.55 (per *ACI 440.1R*); M_{DL} and M_{LL} are the dead and live load moments, respectively. The beam was loaded with a dead load to total load (*D/(D+L)*) ratio of approximately 0.5. Decreasing this ratio did not change results, while increasing this ratio beyond 0.5 generally resulted in slight decreases in reliability, as similar to the results found for steel-reinforced beams [51].

5. Results

The RBDO was conducted with an iterative procedure that systematically increments through feasible sets of DV values to find the minimum cost solution. The process is implemented in two stages, where first a set of feasible bar configurations is developed considering DVs $v_{1\text{-}4}$, as appropriate for bar type, acting on constraints $\sum_{i=1}^{n} v_i = 1.0$ and a constraint similar to $M_{i+1} \geq M_i$ per eq. 6, but based on bar force rather than section moment. Here the volume fractions v_i are incremented at 1% increments. Once a set of feasible bar designs is developed, a set of feasible reinforced concrete flexural members is developed by incrementing through combinations of the remaining DVs (A_{FRP}, *b, h, d*, and f_c') in conjunction with the set of feasible bar designs, and including evaluation of the constraints given in eq (6) found to be critical. In the procedure, A_{FRP} increments at 1.0 mm^2 for beams and 0.1 mm^2 for decks; *b* and *h* increment at 12.7 mm (0.5 in); *d* increments at 6 mm (0.25 in); and f_c' increments at 3.5 MPa (500 psi). Of the set of feasible sections developed, the minimum cost design is then

selected. Although computationally expensive, this method was found to be more stable than a gradient-based solver such as sequential quadratic programming (SQP), which encounters difficulties computing numerical derivatives with the discrete values allowed for the DVs. The accuracy of the optimized solutions using the incremental approach was verified with a series of nonlinear test problems with exact solutions known, with no significant differences in results found [55]. An alternative approach is to use traditional continuous rather than discrete DVs, which would allow numerical compatibility with traditional gradient based methods, then rounding the DV values to the closest increments allowed for the DVs to report a final solution. This computational effort-saving approach was ultimately not used to avoid discrepancies in the calculated RBDO solution and that chosen for the final optimized designs.

Characteristics of optimized flexural members are given in Tables 5a and 5b; Figure 2 presents the stress-strain diagram for the 6 m (20 ft) building beam case bars (other cases are similar), while Figures 3-6 are the moment-curvature responses of all cases considered. For a given bar type (*B1, B2*, or *B3*), little difference was found in optimal bar construction among the different applications considered, where the optimal two material bar (*B1*) was found to be composed of approximately equal quantities of IMCF and AKF-II in each case (v=0.27 each), with about 45% resin. The optimal three material bar (*B2*) was found to be composed primarily of AKF-II (v=0.27), IMCF (v=0.21), and SMCF (v=0.06), with 46% resin. The four material bar (*B3*) was composed of EGF (v=0.21), IMCF (v=0.20), AKF-II (v=0.08) for decks but AKF-I for beams, SMCF (v=0.07), and 44% resin. Optimized reinforcement ratios ranged from 0.0026-0.0036 for decks and from 0.0035-0.0052 for beams, with beams with bars *B1* and *B2* having the highest ratios. Beam depth was found to increase as beam span increased, although no pattern to beam depth was associated with the bridge decks. This is likely because a practical lower limit

of deck thickness was imposed in the problem, which was more than adequate for all cases. No discernable patterns were found with respect to beam width nor area of reinforcement. The relationship between beam depth and width, concrete strength, and area of reinforcement is complex and inter-related, however, as the effect of their combination affects both strength and ductility. All beam optimizations maximized concrete strength, while concrete strength was found to increase as girder spacing increased for the bridge decks.

For every case, all design constraints were met. Tables 6 and 7 provide constraint values for the optimized sections, where the resulting reliability index (β), ratio of design moment capacity to design load ($\phi M_n / M_u$), ductility index (μ_ϕ), ratio of deflection to the deflection limit (Δ / Δ_L), and ratio of reinforcement strain to ultimate strain at beam ultimate flexural capacity, ($\varepsilon_n / \varepsilon_{ult\ n}$), are presented. In all cases, the governing constraint was design moment capacity ($\phi M_n / M_u$), while reliability was somewhat higher than the minimum 3.5 required, varying from approximately 3.8-3.9. For each application, ductility index varied from the minimum imposed (3.0) for case *B1*, to slightly over 3 for case *B2*, to 5.0 for case *B3*. Note that based on the material properties considered, the resulting ductility indices resulted in sections with tension reinforcement strain ε_t significantly higher (approximately $0.02 < \varepsilon_t < 0.04$) at concrete crushing than that required by *ACI 318* for tension controlled steel-reinforced sections ($\varepsilon_t \geq 0.005$).

In no case was the deflection limit a critical concern, although deck deflections were much closer to the limit imposed (with Δ / Δ_L ratios approaching 0.80 for the larger girder spacing considered) than for beams. This is expected, given that the decks have larger span/depth ratios. As seen in the tables, other than differences in deflection limit ratio, however, the specific

application evaluated had little impact on the results, while DHFRP bar type (*B1, B2*, or *B3*) was much more influential.

Table 8 provides a comparison of optimized bar costs, where the specific costs for each application are calculated per eq. 4, then normalized to the lowest cost result for comparison. Here relative costs are compared in two ways: in unit and total costs. Unit costs (cost/bar unit volume) are normalized to the lowest cost found across all applications, which was the *B3* case for the 6 m (20 ft) beam span. The highest unit cost was found in the unoptimized designs (*B1*) for every application, as discussed further below. The total cost comparison considers the amount of reinforcement used in the application as well; i.e. the specific cost multiplied by the bar cross-sectional area. This accounts for fact that some bar designs have inherently less strength than others, and correspondingly require a larger bar area to carry the same tensile force. For reasonable comparisons, total costs are normalized within each of the four applications (i.e. for each of the two deck and beam spans), as some applications require more tensile force to develop the required moment capacity than others. Thus, each application will have a different least total cost case, identified by a total relative cost of 1.0 in Table 8. Also shown in Table 8 are costs relative to traditional steel, given in parentheses. Clearly, DHFRP is much more costly, with the cheapest optimized results (*B3* case bars) from about 10-12 times that of steel. This is primarily due to the need for an expensive IMCF material (Table 1) to enable the bar to meet all performance criteria. The resulting DHFRP bars are approximately twice as expensive as traditional, single-material CFRP bars that use lower grade carbon fibers [3].

In the table, results are presented for unoptimized and the final optimized designs. The unoptimized design is presented for comparison. It represents a reasonable starting design that meets most constraints (all except ductility and reinforcement strain limit). Here, a reasonable

starting design was made for each bar type and used for all applications; hence relative unit costs are identical for a given bar type for each application. It was found that the optimized designs were significantly less expensive than the base designs, generally resulting from a 10 - 30% reduction in relative total costs. In every application, bar costs decreased as the number of materials increased from 2 to 4, where the least costly bars were *B3*. The final optimized bar stress-strain and section moment curvature diagrams are shown in Figures 2 and 3, respectively.

6. Conclusions

A RBDO was conducted on three types of DHFRP reinforcing bars, which were cost-minimized for different bridge deck and building beam design scenarios considering strength, deflection, ductility, and reliability constraints. It was found that, for a given bar type, there was little difference in optimal bar construction among the different applications considered. It was also found that the optimized designs were approximately 10-30% less expensive than the base designs considered, a potentially important cost savings given the relatively expensive material costs involved with DHFRP bar construction. For all cases, bar material costs decreased as the number of materials used in bar construction increased from 2 to 4. It was also found that for all cases, the governing constraint was design moment capacity.

With careful selection of bar material properties and proportions, all DHFRP-reinforced flexural members considered could meet code-specified (i.e. *AASHTO LRFD* as well as *ACI 318*) strength and ductility requirements for steel-reinforced sections. Note that selection of bar and section properties to meet all of the imposed constraints is in general difficult without use of a formal optimization procedure. Although *ACI 440.1R* allows either over or under-reinforced designs with FRP bars, only tension-controlled sections were considered in this study. This is

appropriate, as it only makes sense to use DHFRP bars in tension-controlled members, where bar ductility could be taken advantage of in the case of an overload.

Since the reliability of DHFRP-reinforced flexural members (from approximately β=3.8 to 3.9) was found to be higher than the targets set for steel-reinforced sections considered in this study (β=3.5) , it may be argued that an increase in the allowable resistance factor given by *ACI 440.1R* of 0.55 may be warranted. However, due to other performance differences between DHFRP and steel, such as the inability of the DHFRP-reinforced section to behave in a ductile manner for more than a single overload, which is clearly disadvantageous for cyclic forces, the existing higher level of reliability may be appropriate.

Although strength and ductility requirements can be addressed, an additional consideration with the use of DHFRP, as well as non-ductile FRP bars, is cracked section stiffness for cost-effective bar configurations. It was found that otherwise identical steel-reinforced sections generally have approximately half the deflection as those reinforced with DHFRP bars. As the effective elastic modulus of DHFRP reinforcement is lower than that of steel, deeper sections as well as higher concrete strengths are generally required to simultaneously meet strength, ductility, as well as deflection constraints.

REFERNCES

[1] Federal Highway Administration. Long Term Effectiveness of Cathodic Protection Systems on Highway Structures. Publication No. FHWA-RD-01-096. McLean, VA: FHWA; 2001.

[2] Smith, J.L. and Virmani, P.Y. Performance of Epoxy-Coated Rebars in Bridge Decks. Public Roads 1996; 60(2).

[3] Eamon, C., Jensen, E., Grace, N., and Shi, X. Life Cycle Cost Analysis of Alternative Bridge Reinforcement Materials for Bridge Superstructures Considering Cost and Maintenance Uncertainties. ASCE Journal of Materials in Civil Engineering 2012; 4(24): 373-380.

[4] American Association of State and Highway Transportation Officials. AASHTO LRFD Bridge Design Specifications, 5th ed. Washington, D.C.: AASHTO; 2010.

[5] American Concrete Institute. Building Code Requirements for Structural Concrete and Commentary, ACI 318-11. Farmington Hills, MI: ACI 2011.

[6] American Concrete Institute. Guide for the Design and Construction of Structural Concrete Reinforced with FRP Bars, ACI 440.1R-06. Farmington Hills, MI: ACI; 2006.

[7] American Association of State and Highway Transportation Officials. AASHTO LRFD Bridge Design Guide Specifications for GRFP-Reinforced Concrete Bridge Decks and Traffic Railings. Washington, D.C.: AASHTO; 2009.

[8] Canadian Standards Association. Canadian Highway Bridge Design Code, CSA-S6-06. Toronto, Canada: CSA; 2006.

[9] The International Federation for Structural Concrete. *fib* Bulletin No. 40, FRP Reinforcement in RC Structures, Lausanne, Switzerland: *fib*; 2007.

[10] Japan Society of Civil Engineers. Recommendation for Design and Construction of Concrete Structures using Continuous Fiber Reinforcing Materials, Concrete Engineering Series 23. Tokyo, Japan: JSCE; 1997.

[11] British Standards Institution. Performance Guidelines for Design of Concrete Structures using Fibre-reinforced Polymer Materials, BS ISO 14484. London, UK: BSI; 2011.

[12] Canadian Standards Association International. Design and Construction of Building Components with Fibre-Reinforced Polymers, CSA-S806-02 (R2007). Toronto, Canada: CSA; 2002.

[13] Canadian Network of Centers of Excellence on Intelligent Sensing for Innovative Structures. ISIS Design Manual No. 3 – Reinforcing Concrete Structures with Fibre Reinforced Polymers (FRPs). Manitoba, Canada: ISIS Canada Corp; 2001.

[14] Terry, K.C. Behavior of concrete beams reinforced with hybrid FRP composite rebars. MS Thesis. Hong Kong University of Science and Technology, Dept. of Civil Engineering; 2006.

[15] Tamuzs, V. and Tepfers, R. Ductility of non-metallic hybrid fiber composite reinforcement for concrete. Proceedings of the Second International RILEM Symposium, Ghent, Belgium 1995.

[16] Harris, H.H., Somboonsong, W., and Ko, Frank K. New Ductile Hybrid FRP Reinforcing Bar for Concrete Structures. ASCE Journal of Composites for Construction 1998; 2(1): 28-36.

[17] Bakis, E.C., Nanni, A., and Terosky, J.A. Self-monitoring, pseudo-ductile, hybrid FRP reinforcement rods for concrete applications. Composite Science Technology 2001; 61: 815-823.

[18] Belarbi, A., Watkins, S.E., Chandrashekhara, K., Corra, J., and Konz, B. (2001). Smart fiber-reinforced polymer rods featuring improved ductility and health monitoring capabilities. Smart Materials and Structures 2001; 10(3): 427-431.

[19] Cheung, M. and Tsang, T. Behaviour of Concrete Beams Reinforced with Hybrid FRP Composite Rebar. Advances in Structural Engineering 2010; 13(1): 81-93.

[20] Won, J-P, Park, C-G, and Jang, C-I. Tensile Facture and Bond Properties of Ductile Hybrid FRP Reinforcing Bars. Polymers & Polymer Composites 2007; 15(1): 9-16.

[21] Cui, Y-H and Tao, J. A new type of ductile composite reinforcing bar with high tensile elastic modulus for use in reinforced concrete structures. Canadian Journal of Civil Engineering 2009; 36: 672-675.

[22] Wierschem, N. and Andrawes, B. Superelastic SMA-FRP composite reinforcement for concrete structures. Smart Materials and Structures 2010; 19.

[23] Shield, C.K., Galambos, T.V., and Gulbrandsen, P. On the History and Reliability of Flexural Strength of FRP Reinforced Concrete Members in ACI 440.1R. ACI Publication SP-275. In: Sen, R., Seracino, R., Shield, C., and Gold, W. editors. Fiber-Reinforced Polymer Reinforcement for Concrete Structures, Farmington Hills, MI: American Concrete Institute; 2011.

[24] Ribeiro, S.E.C., and Diniz, S.M.C. Strength and reliability of FRP-reinforced concrete beams. Proceedings of the Sixth International Conference on Bridge Maintenance, Safety and Management 2012: 2280-2287.

[25] Plevris N., Triantafillou T.C., and Veneziano D. Reliability of RC Members Strengthened with CFRP Laminates. ASCE Journal of Structural Engineering 1995; 121(7): 1037–44.

[26] Okeil A.M., El-Tawil S, and Shahawy M. Flexural reliability of reinforced concrete bridge girders strengthened with carbon fiber-reinforced polymer laminates. ASCE Journal of Bridge Engineering 2002; 7(5): 290–299.

[27] Monti, G. and Santini, S. Reliability-Based Calibration of Partial Safety Coefficients for Fiber-Reinforced Plastic. ASCE Journal of Composites for Construction 2002; 6: 162-167.

[28] Zureick, A-H., Bennett, R. M., and Ellingwood, B. R. Statistical characterization of FRP composite material properties for structural design. ASCE Journal of Structural Engineering 2006; 132(8): 1320–1327.

[29] Atadero, R. and Karbhari, V. Calibration of resistance factors for reliability based design of externally-bonded FRP composites. Composites Part B 2008; 39: 665-679.

[30] Wang, N., Ellingwood, B., and Zureick, A-H. Reliability-Based Evaluation of Flexural Members Strengthened with Externally Bonded Fiber-Reinforced Polymer Composites. 2010; 136: 1151-1160.

[31] Wieghaus, K. and Atadero, R. Effect of Existing Structure and FRP Uncertainties on the Reliability of FRP-Based Repair. Journal of Composites for Construction 2011; 15: 635-643.

[32] Ceci, A., Casas, J., and Ghosen, M. Statistical analysis of existing models for flexural strengthening of concrete bridge beams using FRP sheets. Construction and Building Materials 2012; 27: 490-520.

[33] Behnam, B. and Eamon, C. Resistance Factors for Ductile FRP-Reinforced Concrete Flexural Members. ASCE Journal of Composites for Construction (in press).

[34] Hognestad, E. Inelastic Behavior in Tests of Eccentrically Loaded Short Reinforced Concrete Columns. ACI Journal Proceedings 1952; 24(2): 117-139.

[35] Bank, L.C. Composites for Construction Structural Design with FRP Materials. Wiley; 2006.

[36] Naaman, A. E., and Jeong, S. M. Structural Ductility of Concrete Beams Prestressed with FRP Tendons. Proceedings of the Second International RILEM Symposium, Ghent, Belgium, 1995: 1466-1469.

[37] Maghsoudia, A.A., and Bengarb, H.A. Acceptable Lower Bound of The Ductility Index and Serviceability State of RC Continuous Beams Strengthened with CFRP Sheets. Scientia Iranica 2011; 18: 36–44.

[38] Shin, S., Kang, H., Ahn, J., and Kim, D. Flexural Capacity of Singly Reinforced Beam with 150 MPa Ultra High-Strength Concrete. Indian Journal of Engineering & Materials Science 2010; 17: 414-426.

[39] Branson, D.E. Instantaneous and Time-Dependant Deflections of Simple and Continuous Reinforced Concrete Beams. HPR Report No. 7, Part 1. Auburn, Alabama: Department of Civil Engineering and Auburn Research Foundation, Auburn University; 1965.

[40] Branson, D.E. Deformation of Concrete Structures. New York: McGraw-Hill; 1977.

[41] Bischoff, P. H. Deflection Calculation of FRP Reinforced Concrete Beams Based on Modifications to the Existing Branson Equation. Journal of Composites for Construction, ASCE 2007; 11(1).

[42] Bank, L.C., Oliva, M.G., Russell, J.S., Jacobson, D.A., Conachen, M, Nelson, B, and McMonigal, D. Double-Layer Prefabricated FRP Grids for Rapid Bridge Deck Construction: Case Study. Journal Of Composites For Construction 2006; 10(3): 204-212.

[43] Janney, M., Geiger, E., and Baitcher, N. Fabrication of Chopped Fiber Preforms by the 3-DEP Process. American Composites Manufacturers Association. Composites & Polycon; 2007.

[44] Rao, S.S. Reliability-Based Design, New York: McGraw-Hill; 1992.

[45] Enevoldsen, I. and Sorensen, J. D. Reliability-Based Optimization in Structural Engineering. Structural Safety 1994; 15: 169-196.

[46] Frangopol, D. M. Reliability-Based Optimum Structural Design. In: Sundararajan, C., editor. Probabilistic Structural Mechanics Handbook, Theory and Industrial Applications; 1995.

[47] Tu, J., Choi, K. K., and Park, Y. H. A New Study on Reliability Based Design Optimization. Journal of Mechanical Design 1999; 121(4): 557–564.

[48] Eamon, C, and Rais-Rohani, M. Integrated Reliability and Sizing Optimization of a Large Composite Structure. Marine Structures 2009; 22(2): 315-334.

[49] Rais-Rohani, M, Solanki, K, Acar, E., and Eamon, C. Shape and Sizing Optimization of Automotive Structures with Deterministic and Probabilistic Design Constraints. International Journal of Vehicle Design 2010; 54(4): 309-338.

[50] Nowak, A.S. Calibration of LRFD Bridge Design Code. NCHRP Report 368. Washington, D.C.: Transportation Research Board; 1999.

[51] Szerszen, M.M. and Nowak, A.S. Calibration of design code for buildings (ACI 318): Part 2 - Reliability analysis and resistance factors. ACI Structural Journal 2003; 100(3): 383-391.

[52] Nowak, A.S. and Szerszen, M.M. Calibration of design code for buildings (ACI 318): Part 1 – Statistical Models for Resistance. ACI Structural Journal 2003; 100(3): 377-382.

[53] Eamon, C. and Rais-Rohani, M. Structural Reliability Analysis of Advanced Composite Sail. SNAME Journal of Ship Research 2008; 52(3): 165-174.

[54] Berg, A.C., Bank, L.C., Oliva, M.G., Russell, J.S. Construction and cost analysis of an FRP reinforced concrete bridge deck. Construction and Building Materials 2006; 20(8): 515–526.

[55] Behnam, B. Reliability Model for Ductile Hybrid FRP Rebar Using Randomly Dispersed Chopped Fibers. PhD Dissertation. Detroit, MI: Wayne State University, Dept. of Civil and Environmental Engineering; 2012.

Table 1. DHFRP Bar Material Properties

Label	Material	E GPa (ksi)	ε_{u*}	Density, g/cc (lbs/ft^3)	Specific cost
IMCF	IM-Carbon Fiber	400 (58000)	0.0050	1.76 (110)	50
SMCF	SM-Carbon Fiber	238 (34500)	0.0150	1.76 (110)	6.0
AKF-I	Aramid Kevlar-49 Type I	125 (18000)	0.0250	1.45 (91)	8.0
AKF-II	Aramid Kevlar-49 Type II	102 (15000)	0.0250	1.45 (91)	8.0
EGF	E-Glass fiber	74 (11000)	0.0440	2.56 (160)	1.0
Resin	Epoxy	3.5 (540)*	0.0600	1.05 (66)	1.5

*Shear modulus G is taken as 1.26 MPa (194 ksi)

Table 2. Design Variables

DV	Description	Lower Bound*	Upper Bound
v_i (i=1-4)	Material volume fraction	0.05	1.0
A_{FRP}**	Reinforcement area, mm^2 (in^2)	15; 650 (0.002; 1.0)	--
f_c'	Concrete strength, MPa (ksi)	31 (4.5)	38 (5.5)
b	Beam width, mm (in)	460 (18)	560 (22)
d***	Reinforcement depth, mm (in)	180; 570; 880	230; 830; 1270
		(7, 22.5, 34.5)	(9, 32.5, 50)

*Also the initial value for the DV. **Values provided for deck and beam cases, respectively.
***Values provided in order for: deck; 6 m (20 ft) span beam; 9.1 m (30 ft) span beam.

Table 3. Resistance Random Variables

RV*	Description	V	λ
$v_{\text{IM-Carbon}}$	Volume fraction of IM-Carbon	0.05	1.00
$v_{\text{SM-Carbon}}$	Volume fraction of SM-Carbon	0.05	1.00
$v_{\text{Kevlar}-49}$	Volume fraction of Kevlar-49	0.05	1.00
$v_{E-Glass}$	Volume fraction of E-Glass	0.05	1.00
v_{resin}	Volume fraction of resin	0.05	1.00
$E_{\text{IM-Carbon}}$	Modulus of elasticity of IM-Carbon	0.08	1.04
$E_{\text{SM}-\text{Carbon}}$	Modulus of elasticity of SM-Carbon	0.08	1.04
$E_{\text{Kevlar}-49}$	Modulus of elasticity of Kevlar-49	0.08	1.04
$E_{E-glass}$	Modulus of elasticity of E-glass	0.08	1.04
E_{resin}	Modulus of elasticity of resin	0.08	1.04
ε_{f_1}	Failure Strain of IM-Carbon	0.05	1.20
f_c'	Compressive strength of concrete		
	Bridge slab	0.04	1.14
	Building beam	0.05	1.14
d	Depth of reinforcement		
	Bridge slab	0.10	0.94
	Building beam	0.04	0.99
b	Building beam width	0.04	1.01
P	Professional factor	0.16	0.89

*All distributions are normal.

Table 4. Load Random Variables

RV*	Description	V	λ
Bridge Slab			
DS	Dead load, slab	0.10	1.05
DW	Dead load, wearing surface	0.25	1.00
DP	Dead load, parapet	0.10	1.05
LL	Truck wheel load	0.18	1.20
Building Beam			
DL	Dead load	0.10	1.00
LL	Live load	0.18	1.00

*All distributions are normal except live loads, which are extreme type I.

Table 5a. Design Variable Results for Optimized Deck Sections

	Girder Spacing:	1.8 m			2.7 m		
DV	DV material	*B1*	*B2*	*B3*	*B1*	*B2*	*B3*
v_1	IMCF	0.27	0.21	0.20	0.27	0.21	0.21
v_2	SMCF	-	0.06	0.07	-	0.06	0.07
v_3	AKF-I	-	-	-	-	-	-
v_3	AKF-II	0.29	0.27	0.08	0.29	0.27	0.09
v_4	EGF	-	-	0.21	-	-	0.20
v_r	Resin	0.44	0.46	0.44	0.44	0.46	0.43
A_{FRP}*	(mm^2)	160	175	160	200	220	215
d	(mm)	200	180	200	200	200	210
f_c'	(MPa)	28	28	31	31	31	35

*per 300 mm (12 in) deck width

Table 5b. Design Variable Results for Optimized Beam Sections

		Span 6 m			Span 9.1 m		
DV	DV material	*B1*	*B2*	*B3*	*B1*	*B2*	*B3*
v_1	IMCF	0.26	0.21	0.20	0.26	0.21	0.21
v_2	SMCF	-	0.06	0.07	-	0.07	0.07
v_3	AKF-I	-	-	0.07	-	-	0.07
v_3	AKF-II	0.29	0.26	-	0.29	0.27	-
v_4	EGF	-	-	0.21	-	-	0.21
v_r	Resin	0.45	0.47	0.45	0.45	0.45	0.44
A_{FRP}	(mm^2)	1550	1610	1290	2520	2390	2190
b	(mm)	460	460	460	530	520	560
d	(mm)	650	685	850	900	980	1110
f'_c	(mPa)	38	38	38	38	38	38

Table 6. Constraint Evaluation Results for Deck

	B1	*B2*	*B3*
Girder Spacing L=1.8 m (6 ft)			
β	3.92	3.92	3.92
$\phi M_n/M_u$	1.0	1.0	1.0
μ_ϕ	3.0	3.04	5.0
Δ/Δ_L	0.33	0.51	0.47
$\varepsilon_n/\varepsilon_{ult\ n}$	0.97	0.98	0.85
Girder Spacing L=2.7 m (9 ft)			
β	3.90	3.92	3.94
$\phi M_n/M_u$	1.0	1.0	1.0
μ_ϕ	3.0	3.1	5.0
Δ/Δ_L	0.79	0.73	0.65
$\varepsilon_n/\varepsilon_{ult\ n}$	1.0	1.0	0.85

Table 7. Constraint Evaluation Results for Beam

	B1	*B2*	*B3*
Beam Span L=6 m (20 ft)			
β	3.75	3.79	3.94
$\phi M_n/M_u$	1.0	1.0	1.0
μ_ϕ	3.0	3.4	5.0
Δ/Δ_L	0.045	0.041	0.029
$\varepsilon_n/\varepsilon_{ult\ n}$	0.86	0.91	1.0
Beam Span L=9.1 m (30 ft)			
β	3.76	3.71	3.92
$\phi M_n/M_u$	1.0	1.0	1.0
μ_ϕ	3.0	3.3	5.0
Δ/Δ_L	0.048	0.044	0.035
$\varepsilon_n/\varepsilon_{ult\ n}$	0.86	0.94	1.0

Table 8. Optimized Normalized Bar Costs

	Unoptimized Designs		Optimized Designs	
Section	Relative Unit Cost	Relative Total Cost	Relative Unit Cost	Relative Total Cost
Deck, 1.8 m (6 ft) Girder Spacing				
B1	1.60 (16.2)	1.91 (20.8)	1.38 (13.9)	1.70 (18.5)
B2	1.38 (13.9)	1.65 (18.0)	1.16 (11.7)	1.24 (13.5)
B3	1.17 (11.8)	1.40 (15.3)	1.01 (10.2)	1.00 (10.9)
Deck, 2.7 m (9 ft) Girder Spacing				
B1	1.60 (16.2)	1.58 (19.3)	1.58 (15.5)	1.29 (15.7)
B2	1.38 (13.9)	1.36 (16.6)	1.36 (13.7)	1.18 (14.4)
B3	1.17 (14.2)	1.16 (14.2)	1.16 (11.7)	1.00 (12.2)
Beam, 6 m (20 ft) Span				
B1	1.60 (16.2)	2.00 (23.8)	1.35 (13.6)	1.63 (19.4)
B2	1.38 (13.9)	1.72 (20.5)	1.15 (11.6)	1.44 (17.1)
B3	1.17 (11.8)	1.46 (17.4)	1.00 (10.1)	1.00 (11.9)
Beam, 9.1 m (30 ft) Span				
B1	1.60 (16.2)	1.67 (20.7)	1.35 (13.6)	1.47 (18.2)
B2	1.38 (13.9)	1.44 (17.9)	1.16 (11.7)	1.21 (15.0)
B3	1.17 (11.8)	1.22 (15.1)	1.04 (10.5)	1.00 (12.4)

Note: values in parentheses represent costs relative to steel.

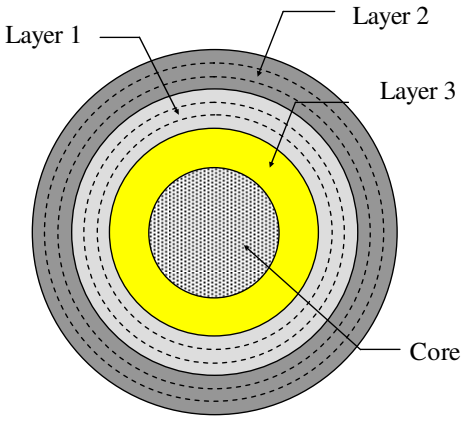

Figure 1. DHFRP Bar Concept

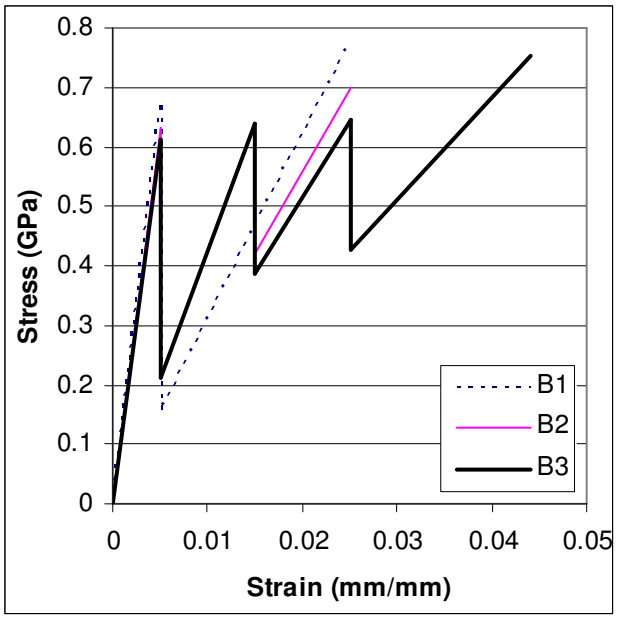

Figure 2. Stress-Strain Curves for DHFRP Bars

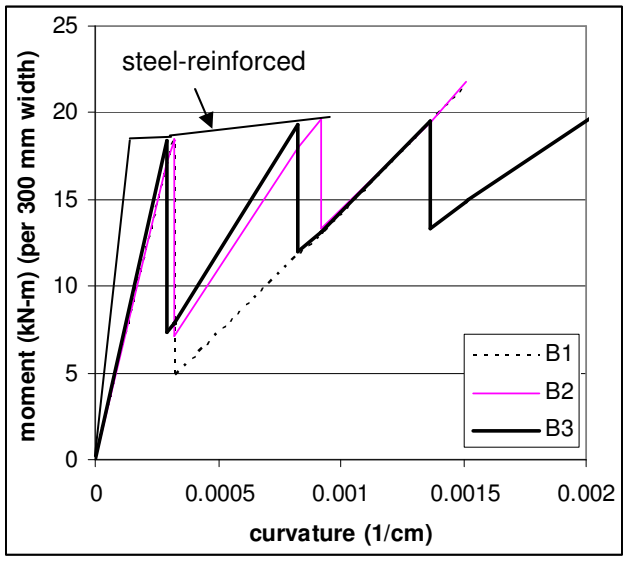

Figure 3. Moment-Curvature Diagram for DHFRP-Reinforced Deck (1.8 m)

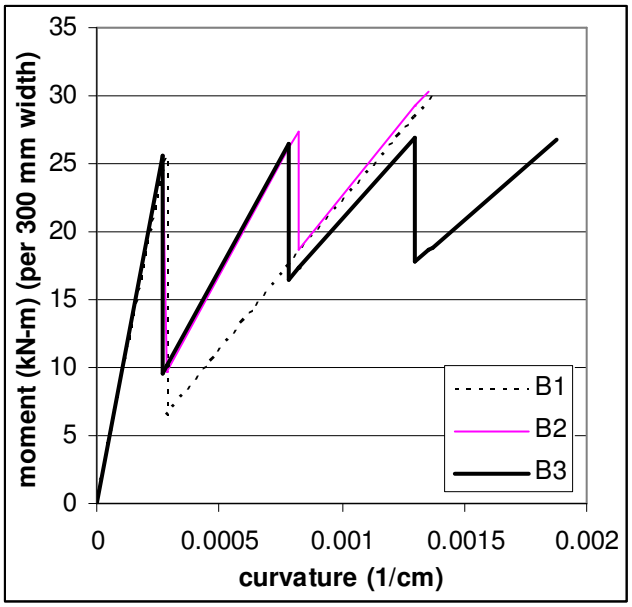

Figure 4. Moment-Curvature Diagram for DHFRP-Reinforced Deck (2.7 m)

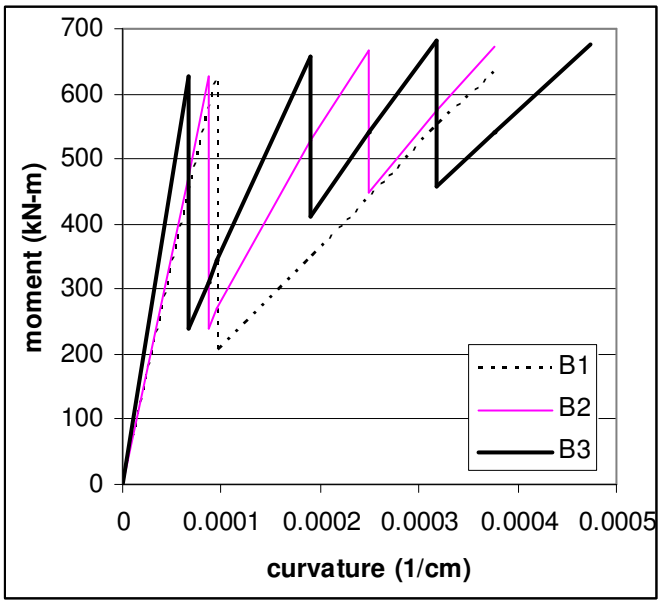

Figure 5. Moment-Curvature Diagram for DHFRP-Reinforced Beam (6 m)

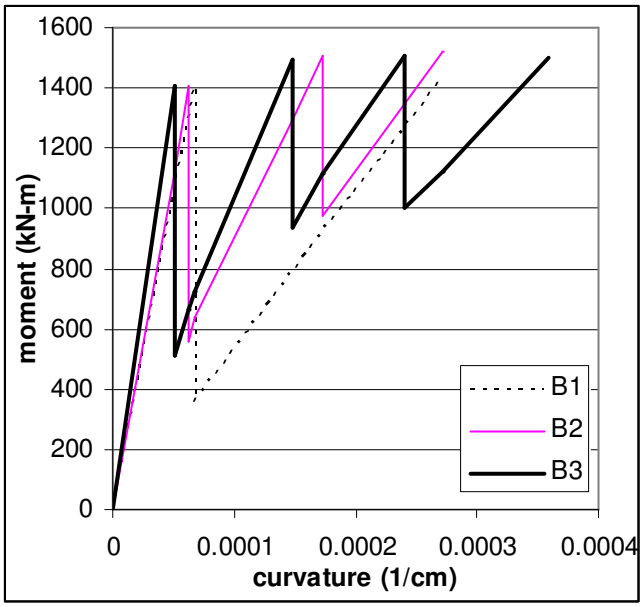

Figure 6. Moment-Curvature Diagram for DHFRP-Reinforced Beam (9 m)

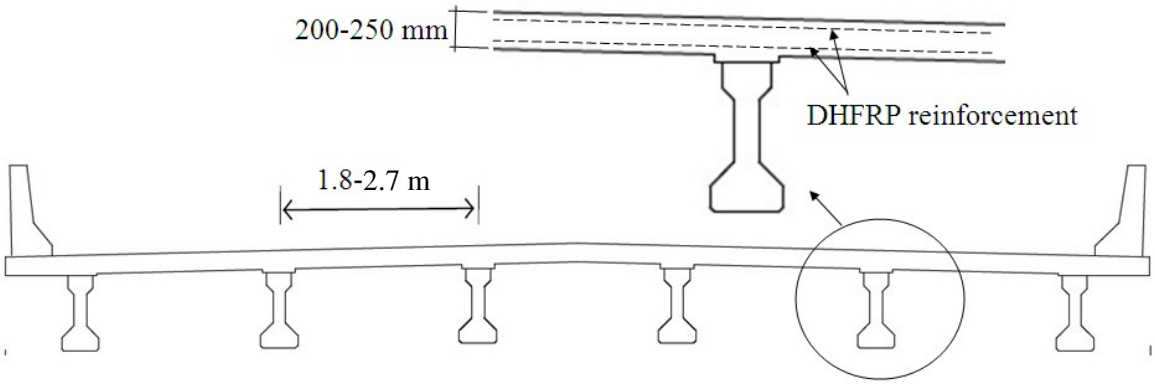

Figure 7. Bridge Deck